A fusion prognostics strategy for fuel cells operating under dynamic conditions

Chu Wang, Manfeng Dou, Zhongliang Li, Rachid Outbib, Dongdong Zhao, Bin Liang

A Fusion Prognostics Strategy for Fuel Cells Operating under Dynamic Conditions

Chu Wang [a, b, *], Manfeng Dou [a], Zhongliang Li [b, c, **], Rachid Outbib [b], Dongdong Zhao [a], Bin Liang [d]

[a] School of Automation, Northwestern Polytechnical University, Xi'an 710072, China

[b] LIS Lab (UMR CNRS 7020), Aix-Marseille University, 13397 Marseille, France

[c] FEMTO-ST (CNRS 6174)/FCLAB (CNRS 3539), 90010 Belfort, France

[d] Department of Automation, Tsinghua University, Beijing 100084, China

[*] Corresponding author: Chu Wang (e-mail: chu.wang@etu.univ-amu.fr)

[**] Corresponding author: Zhongliang Li (e-mail: zhongliang.li@lis-lab.fr)

Abstract

Transportation-oriented proton exchange membrane fuel cells (PEMFC) are attracting much attention, but the strong dynamic operating conditions in transportation applications limit the durability improvement and wide commercialization of fuel cells (FC). Prognostics dedicated to predicting the FC remaining useful life (RUL) can facilitate the early provision of control/maintenance programs to improve durability and reduce costs. However, credible degradation indexes for prognostics are difficult to access or observe directly from the FC operating under dynamic conditions. Moreover, the long-term prediction performance of the state-of-the-art prognostics models is often not satisfactory. This paper proposes a fusion prognostics strategy to address these challenges. Specifically, the system dynamics is identified by using an electrochemical mechanism model and the degradation indexes are extracted based on the identified model parameters. Subsequently, a reduced-dimensional symbolic representation based long short-term memory network is developed for predicting the evolution of degradation. The proposed approach is validated using the long-term accelerated stress test data of a vehicle-oriented PEMFC. The results show that the degradation mechanism model can be used to identify degradation indexes in dynamic operating conditions. Based on the prognostics model, accurate RUL prediction can further be achieved over the extracted degradation indexes.

Keywords: Proton exchange membrane fuel cells;

Dynamic conditions;

Electrochemical degradation model;

Degradation indexes;

Failure range;

Remaining useful life

1 Introduction

Recently, there is an exponential growth in the focus on all clean energy sources. This comes partly from the distress caused by the fossil fuel shortage and, more seriously, from the exhaust emissions of combustion. Further, reducing carbon emissions in industrial processes and transportation is urgent but challenging [1]. Fuel cells (FC) are expected to alleviate this challenge, thanks to their operation without onboard CO_2 emissions and air pollution [2]. In particular, proton exchange membrane fuel cells (PEMFC) exhibit

advantages such as high power density, low starting/running temperature, and high energy conversion efficiency. This allows PEMFC to be suitable for diverse transportation applications, e.g., hybrid/plug-in hybrid vehicles [3,4], heavy-duty trucks [1], buses [5], trains [6], ships [7]. However, the large-scale commercialization of PEMFC still has to face the challenges of durability improvement and cost reduction [8]. For instance, the durability of fuel cells used for low-duty automotive is currently less than 5,000 hours, while the ultimate goal is targeted at 8,000 hours by 2025 [1].

Prognostics and health management (PHM) has the ability to improve FC durability and is considered as one of the superior solutions [9]. In PHM, the accuracy of prognostics plays a deterministic role in the timing of maintenance/control deployment and affects the effectiveness of health management. Prognostics provides the basis for the "Predict"–"Maintain" strategy considered as an alternative of the "Failure"-"Replace" strategy [10]. The former is considered to be better not only to improve the durability but also to reduce the maintenance cost [11]. The International Organization for Standardization (ISO) defines prognostics as "analysis of the symptoms of faults to predict future condition and residual life within design parameters" [12]. Accordingly, for FC ageing prognostics, the core task involves refining the degradation index (DI), predicting the state of health (SoH) and/or the remaining useful life (RUL) [13]. For FC operating in constant conditions, some measurements (such as stack voltage [14,15,16]) can be directly assigned as DI. On the other hand, dynamic operating conditions not only affect the transient response of PEMFC performance [33], but also make it difficult to evaluate directly the degradation from measurements. As a result, a suitable DI needs to be extracted for long-term ageing prognostics under dynamic conditions and different DI extraction methods have been studied in the literature [17,18,19,20,21,38,39]. Specifically, Bressel et al. in [17] and Ma et al. in [38], estimate the actual SoH and degenerate dynamics using the extended Kalman filter and select the degeneration model parameters as DI. Mezzi et al. assume constant effects of FC system operating conditions and select periodic dynamic voltages as DI [18]. Li et al. use a linear parameter-varying model to extract the virtual steady-state voltage as DI [19,20]. Yue et al. employ a multiplicative feature decomposition method in [21], and a nonlinear regression method combined with a polarization model in [39], to extract the DI. In general, facing the complex operating conditions in transportation applications, it is still challenging to effectively decouple the system dynamics from the ageing effects and obtain physically interpretable DI.

In the phase of SoH/RUL prediction, the performance of model-free or data-driven based methods is encouraging. This is due to the fact that such methods adeptly learn and predict the trend characteristics of DI [10,13]. In particular, methods in long short-term memory networks (LSTM) framework have demonstrated their strong performance in short-term SoH prediction [14,15,16,22,37]. However, LSTM performance becomes unsatisfactory with increased prediction horizon length which is observed and indicated in our previous work [15,23,36]. Interestingly, the cause of this issue may stem from the powerful "memory" ability of the LSTM, which incorrectly records irrelevant features in the training set. To cope with this issue, Ma et al. in [14] propose to use a fusion model combining the auto-regressive integrated moving average (ARIMA) method with the LSTM. In general, the LSTM based prognostics model still need to be improved in DI long-term prediction while the related studies are extremely limited.

Another key challenge for developing credible FC prognostics tools, especially for PEMFC applied in transportation, is the scarcity of long-term ageing data. A recent review [24] comprehensively reports state-of-the-art durability experimental methods for vehicle-oriented PEMFC. The use of the accelerated stress test (AST) not only enables the assessment of FC lifetime, but also effectively reduces the experimental cost and

time.

To tackle the above issues, this paper proposes a fusion prognostic strategy for PEMFC in transportation applications, consisting of model-based DI extraction and model-free RUL prediction. Specifically, a time-varying degradation model based on the FC electrochemical mechanism is developed to track the load dynamics. The model parameters are identified in variable width intervals, specifying the equivalent resistance and the reconstructed virtual-constant power as DIs, respectively. In the phase of RUL prediction, a reduced-dimensional symbolic representation based LSTM model is used to predict the possible trends of DI. Subsequently, a series of predicted trends form a probability density distribution and RUL is calculated. Finally, the proposed method is validated using a vehicle application-oriented long-term AST dataset.

Sections 2-6 of the article are structured as follows: Section 2 presents the proposed degradation mechanism model. In Section 3, the RUL prediction model and the fusion prognostics strategy are talked about. The experiments used to validate the method are described in Section 4. Section 5 summarizes the prognostic results. The paper is finally concluded in Section 6.

2 Model-based dynamics degradation index extraction

2.1 Degradation mechanism model

Utilizing electrochemical mechanisms such as the models based on polarization curves has been recognized as effective to explain FC voltage losses [25]. The polarization curve model contains the voltage losses due to activation (V_{act}), ohmic (V_r), and concentration (V_{conc}), and is generally expressed as

$$E_{cell} = E_{rev} - v = E_{rev} - V_{act} - V_r - V_{conc} \tag{1}$$

where E_{cell} is the cell voltage, E_{rev} is the reversible open-circuit voltage, v is the global overpotential. A typical polarization curve model is for single cell modelling and generalizes to an n-cell stack level ($E_{stack} = n \cdot E_{cell}$) ignoring inter-cell differences. However, this model is generally suitable for portraying a PEMFC voltage response to static operating conditions and is unable to track transient voltage evolutions in dynamic conditions.

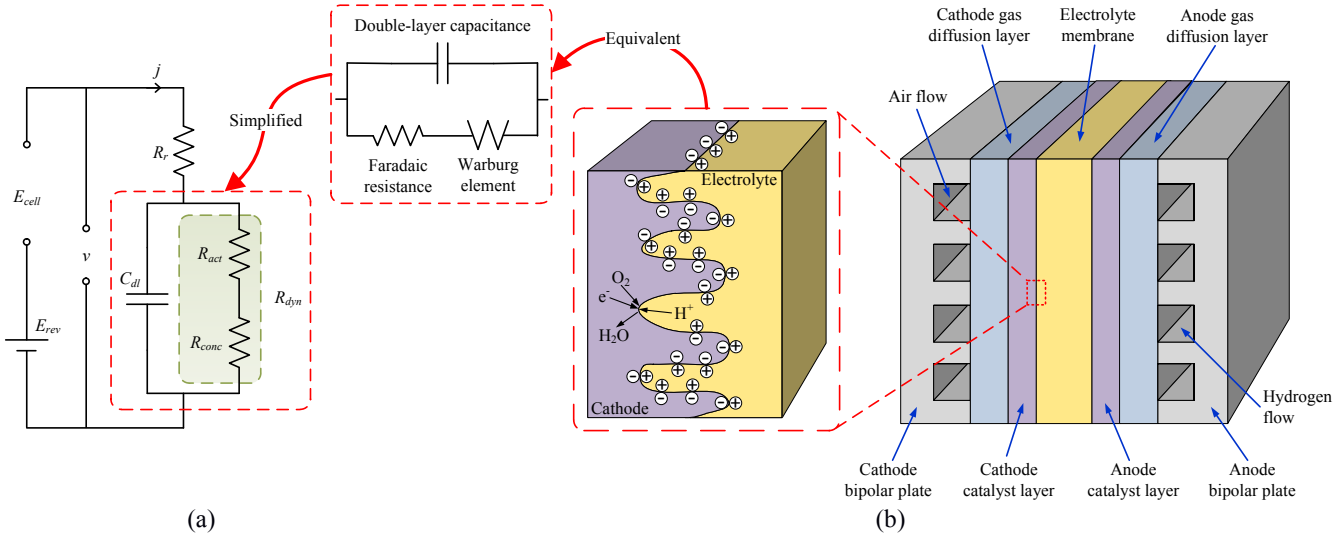

Figure 1. PEMFC electrochemical mechanism schematic:
(a) equivalent circuit model;
(b) physical representation of an electrochemical reaction interface.

A typical electrochemical reaction interface is depicted in Figure 1. The electrochemical characteristics of the reaction interface are represented by using a resistor (R_{dyn}) and a capacitor (C_{dl}) in parallel, as in Figure 1 (a) [26]. Here, R_{dyn} is called the dynamic resistor to quantify the electrochemical reaction dynamic characteristics. Generally, these dynamics include not only the charge transport caused by electrochemical reaction kinetics, but also the mass transport due to reactant/product concentration differences. Further R_{dyn} can be decomposed into two resistors R_{act} and R_{conc}. In this case, R_{act} (a. k. a., Faradaic resistor) models the charge transport, which corresponds to the linear part of the activation overpotential. Similarly, R_{conc} is used to simplify the Warburg element to simulate the mass transport, which corresponds to the linear part of the concentration overpotential [27]. R_r is the resistor corresponding to ohmic losses. Based on this, the three voltage losses can be refined by using the following equations,

$$\begin{cases} V_{act} = \overbrace{jR_{act}}^{\text{linear}} + \overbrace{\dfrac{\mathrm{R}T}{\alpha_{a+c}\mathrm{F}}\ln\left(\dfrac{j+j_{loss}}{j_{exch}}\right)}^{\text{non-linear}} \\ V_R = jR_r \\ V_{conc} = \underbrace{jR_{conc}}_{\text{linear}} - \underbrace{\dfrac{\mathrm{R}T}{\beta_{a+c}\mathrm{F}}\ln\left(\dfrac{j_{max}-j}{j_{max}}\right)}_{\text{non-linear}} \end{cases} \tag{2}$$

where, j is the stack current density, j_{loss} is the crossover current density, j_{exch} is the exchange current density; j_{max} is limiting current density. R is Molar gas constant (8.3145 J/mol/K), F is Faraday constant (96485 C/mol). α_{a+c} is the transfer coefficient, β_{a+c} is a parameter related to the number of electrons transferred in the overall reaction. Both α_{a+c} and β_{a+c} combine the effects of the anode and the cathode. T is the operating temperature (thermodynamic temperature) of the cell. Further, R_r and R_{dyn} are combined as the equivalent resistance (R_{equ}), which represents the overall resistance of the cell, as

$$R_r + R_{act} + R_{conc} = R_r + R_{dyn} = R_{equ} \tag{3}$$

In addition, C_{dl} is called the double-layer capacitor, which corresponds to the capacitance characteristics of the reaction interface. As in Figure 1(b), in the electrochemical reaction, significant charge separation occurs at the reaction interface, with electrons and ions accumulating respectively on the electrode and electrolyte sides. The reaction interface behaves like a capacitor due to the charge separation phenomenon. As shown in the figure, the electrode/electrolyte interface is not smooth, which makes C_{dl} evident and not ignorable [27].

In general, the output voltage/power shows decreases along with the PEMFC degradation. In the case of the equivalent circuit modelling, as in Figure 1(a), the decrease in E_{cell} can be attributed to the effect of time-varying parameters such as R_r, R_{dyn}, C_{dl} and E_{rev}. These parameters can be candidates for degradation indexes in Section 2.2. There are diverse methods to achieve degradation model parameter identification, such as polarization curve-fitting. The direct use of classical polarization curve-fitting is reliable at constant load conditions. This work aims to identify the dynamic behaviour of the fuel cell, especially at load switching moments. Thus, to identify the time-varying dynamics of the equivalent circuit in Figure 1(a), the following equation is utilized.

$$v(t) + R_{dyn}C_{dl}\frac{dv(t)}{dt} = \left(R_r + R_{dyn}\right)j(t) + R_rR_{dyn}C_{dl}\frac{dj(t)}{dt} \tag{4}$$

Further, the one-sided Laplace transform of the left and right sides of equation (4) can be done to obtain the system transfer function, as

$$H(s) = \frac{V(s)}{J(s)} = \frac{R_r s + \left(R_r + R_{dyn}\right)/\left(R_{dyn}C_{dl}\right)}{s + 1/\left(R_{dyn}C_{dl}\right)} = \frac{b_1 s + b_2}{s + a_1} \tag{5}$$

where $H(s)$ is considered as a single-input, single-output system. a_1 represents the Laplace variable of the denominator polynomial, and b_1 and b_2 represent the Laplace variables of the numerator polynomial. By feeding the data of both temporal input $j(t)$ and output $v(t)$, the model parameters a_1 b_1 and b_2 can be identified. The model parameters R_r, R_{dyn}, C_{dl} and E_{rev} can further be deduced. The parameter identification process is summarized in Appendix A.

2.2 Degradation index extraction based on variable width division

The electrochemical mechanism-based degradation model described above has the ability to characterize the short-term dynamics. Concerning the long-term ageing, the electrochemical characteristics of FC change over time and some ageing-related parameters can be used to reflect the FC long-term evolution. A DI extraction method based on variable width division is therefore proposed in this paper, as in Figure 2. Specifically, the samples of current density, cell temperature and cell voltage within a time slot are set as inputs, while the degradation model parameters are set as model identification outputs among which degradation indexes are further selected. It is worth mentioning that cell temperature has a relationship with the thermal characteristics, and affects the power output performance/degradation behaviour of the stack/system [34]. Considering the generalization of the method, several of the measurements are difficult to obtain in some cases (e.g., dead-ended mode). Moreover, at this moment, air pressure and stoichiometry are highly coupled to temperature [35]. Therefore, the use of cell temperature as an input variable is beneficial to profile the factors affecting durability that are not covered by the electrochemical mechanistic model.

In general, all parameters in Equations (1) to (3) are time-varying except for the Molar gas constant (R) and Faraday constant (F). Identifying all time-varying parameters is beneficial to model fuel cells comprehensively, but leads to higher computational costs and difficulty in practical deployment. One potential solution is to simplify appropriately the model by making some of the variable parameters constant and considering the ageing effects using the remaining variable parameters.

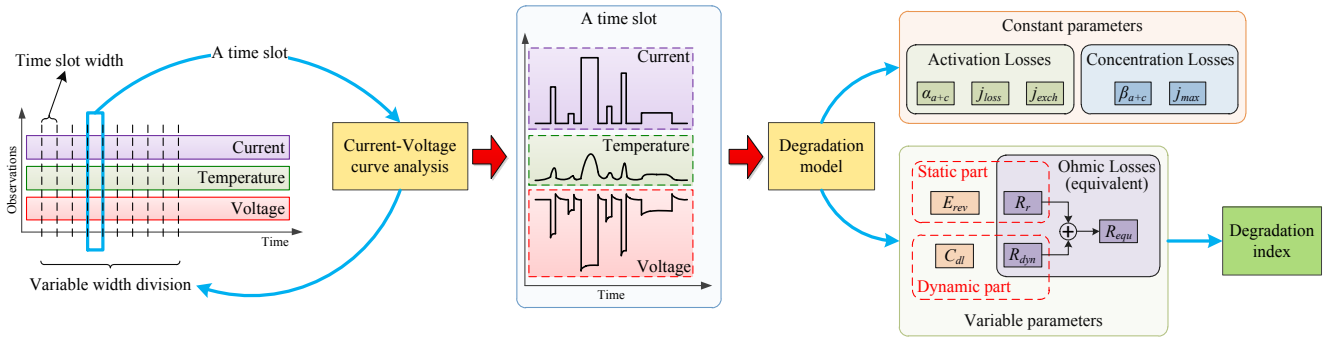

Figure 2. Schematic of variable width division-based degradation index extraction.

As the FC ageing is relatively slow, the ageing-related parameters can be considered constant in short-term time slots (hourly level). The time slot width should be set in the way that the data within the time slot contain sufficient system dynamics for model identification. As shown on the right side of Figure 2, the variable parameters, i.e., E_{rev}, C_{dl}, R_r, and R_{equ} are identified in each time slot via the model identification procedure presented in Appendix A. It is worth mentioning that in some studies (e.g., [9]), the constant parameters considered in this paper are also used to indicate degradation. Nevertheless, most of them are difficult to model precisely or can be considered combined in variable parameters to simplify the model properly. For instance, the impact of degradation on j_{loss} can be reflected and quantified using E_{rev}. Thus, j_{loss} is considered as a constant while E_{rev} is set as a variable parameter.

Once identified, the parameters that demonstrate evident time-varying characteristics can be considered as the candidates for DI. By further analyzing the trendiness/smoothness of the candidates, the DI suitable for prognostics is selected. In addition, it is possible to consider bringing all the identified parameters into equations (1)-(3) and replacing the original dynamic operating current density with a virtual constant current. Accordingly, the virtual steady-state voltage and power can be calculated. It is thus possible to analyze the output power drop as DI at different loads, especially at nominal power/full load.

3 Model-free remaining useful life prediction

3.1 ABBA-LSTM

The Raw-LSTM (a. k. a., Vanilla-LSTM) encounters performance decreasing in long-term prediction, especially when there is a lack of training data concerning the prediction horizon [28]. In the stage of SoH prediction, we use an LSTM model with adaptive Brownian bridge-based aggregation (ABBA-LSTM) to tackle this issue. The core idea is to express the original data with reduced dimensional symbols/letters to improve the sensitivity of Raw-LSTM to trend features. Specifically, ABBA-LSTM can be divided into three parts: representation, prediction, and reconstruction, as in Figure 3.

- Representation:

  There are two steps to go through in this part, (1) Compression: which converts an n-dimensional historical DI (time series X) into an m-dimensional set of segments ($Q \in \mathbb{R}^m$). Next, a time increment (*len*) and a numerical increment (*inc*) of each segment are used to form a tuples-set (D). (2) Digitization: after standardization and scaling, an alphabet set (L) corresponding to k clustering categories is constructed. The tuples in D are expressed using the letters in L to obtain the character series A of length m.

- Prediction:

  In the prediction part, a 5-layer LSTM model is utilized, where the input is the character series A. After two LSTM layers, a fully connected layer and a Softmax layer, the output character series B contains the predictions for p time steps.

- Reconstruction:

  The predicted character series needs to be recovered as a time series before it is used for FC prognostics, and this part is regarded as the inverse process of representation. Converting character series B to predicted time series Y is realized by Inverse-digitization and Inverse-compression.

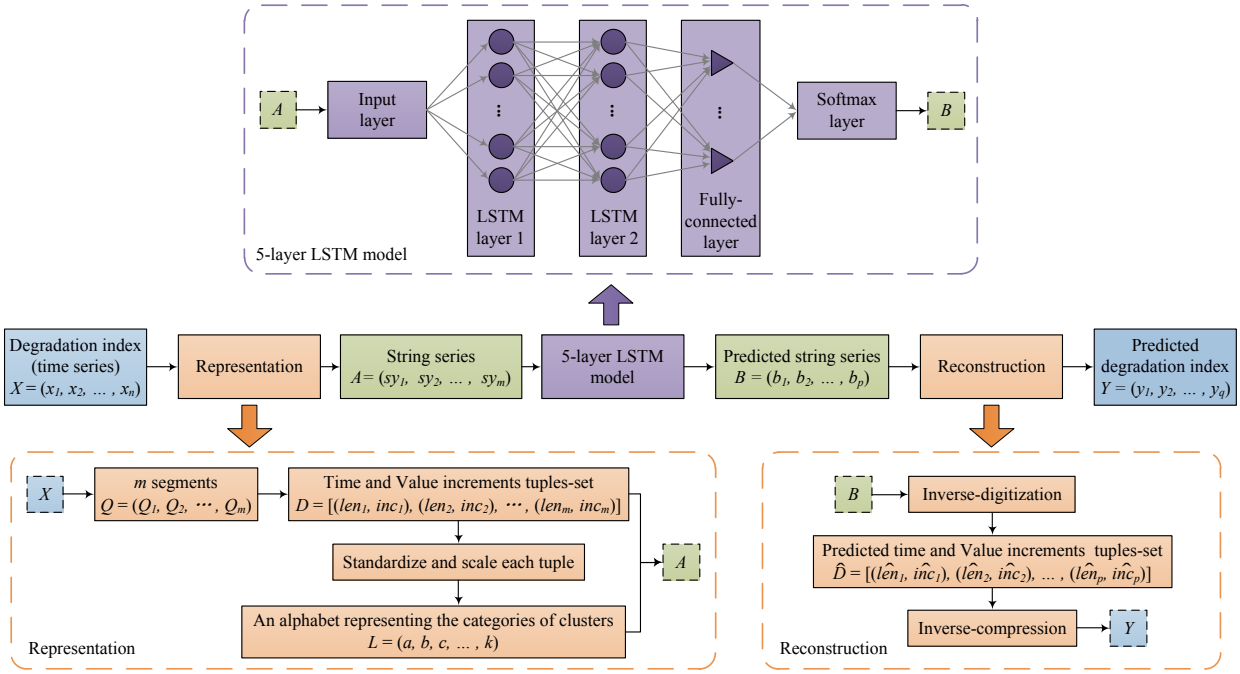

Figure 3. Flowchart of the proposed ABBA-LSTM prognostics model.

To describe this process more clearly, a series of notation marks involved in the ABBA-LSTM prognostics model are shown in Table 1. The detailed operations in each step listed in Figure 3 could be found in our previous work [23].

Table 1 Notation marks during degradation index series conversion

Type	Notation of sets	Remark
Time series	$X = (x_1, x_2, \cdots, x_n) \in \mathbb{R}^n$	Historical degradation index
Compression	$D = \begin{bmatrix} (len_1, inc_1), (len_2, inc_2) \\ , \cdots, (len_m, inc_m) \end{bmatrix} \in \mathbb{R}^{2\times m}$	Time and numerical increment tuples-set
Digitization	$L = (a, b, c, \cdots, k)$	Alphabet set representing clusters' categories
Digitization	$A = (sy_1, sy_2, \cdots, sy_m) \in L^m$, where $sy_i \in L\ (i = 1, \ldots, m)$	m-dimensional character series
Prediction	$B \in L^p$	p-dimensional predicted set of characters
Inverse-digitization	$\widehat{D} \in \mathbb{R}^{2\times p}$	Predicted increments tuples-set
Inverse-compression	$Y \in \mathbb{R}^q$	Predicted degradation index (q time steps)

3.2 Fusion prognostics strategy

The central goal of fusion prognostics is to predict RUL. According to the ISO definition, RUL is the "remaining time before system health falls below a defined failure threshold" [12]. The failure threshold (TF) directly determines the end-of-life (EoL) of fuel cells. In 2011, the U.S. Department of Energy (DoE) defined EoL as a 10% loss of initial performance, which is suitable for constant current operating conditions. However, when a PEMFC operates in dynamic load conditions, there is still no agreement on the definition of the FT [29]. In some cases, different FTs lead to significantly different RULs [24]. Furthermore, desirable FTs should be closely related to the application. It is not optimal to have a single/uniform FT for fuel cells from different applications.

A probable failure range (PFR) and a calculable failure range (CFR) are proposed in this paper. Specifically, as shown in Figure 4 (a), the prediction starting point (t_0) and the extreme point of recoverable fault (t_{limit}) divide the ageing data into three parts: training, prognostics, and invalid data. Before t_0 is considered as the observed historical data (a. k. a., training set), which is used to train the prognostics model. Then between t_0 and t_{limit} is the prognostics zone (a. k. a., test set). It is worth noting that the operation time corresponding to t_{limit} is usually less than or equal to the one corresponding to t_{end}. In the case where t_{limit} is not equal to t_{end}, the part between the two points is defined as invalid data. This is because the performance recovery that occurs after t_{limit} is not sufficiently reliable and may cause serious errors in the prognostics. The range between the expected earliest failure point (t_{a_1}) and the complete failure point (or data ending point, t_{end}) is considered as PFR, and the range between the t_{a_1} and the t_{limit} is considered as CFR.

As a fuel cell runs, fresh observations are constantly acquired. The t_0, which divides the "history" from the "future", will also be updated to deploy the next-round of prognostics. For a particular prediction starting time point, the zoom-in illustration of the prognostic part is shown in Figure 4 (b). By setting *l* random initial weight parameters, the ABBA-LSTM model can output a series of predicted degradation index $\hat{Y} = (Y_1, Y_2, \dots, Y_l)$, where $Y_1, Y_2 \dots Y_l \in \mathbb{R}^q$. The CFR contains *h* failure thresholds $FT = (FT_1, FT_2, \dots, FT_h)$.

- For the *i*-th $(i = 1, 2, \dots, h)$ failure threshold FT_i:

  Based on the degradation index series $\hat{Y}$ and FT_i, a series of RUL (RUL_i) can be calculated as

$$\begin{cases} RUL_i = \left(RUL_{i_1}, RUL_{i_2}, \dots, RUL_{i_j}, \dots, RUL_{i_l}\right) \in \mathbb{R}^l \\ RUL_{i_j} = t_{i_j} - t_0 \\ RUL_{a_i} = t_{a_i} - t_0 \end{cases} \tag{6}$$

  where RUL_{i_j} is the *j*-th $(j = 1,2, \dots, l)$ element in RUL_i. t_{i_j} is the operation time at the crossing point of the *j*-th degradation index Y_j and FT_i. t_{a_i} is the operation time at the crossing point of actual DI and FT_i. RUL_{a_i} is the actual RUL value. Estimate the probability density distribution (P_i) based on the RUL series RUL_i, as

$$f\left(RUL_{P_i}\right) = P_i \tag{7}$$

  where RUL_{P_i} corresponds to the RUL values of the horizontal coordinate of P_i. The final predicted RUL value ($\widetilde{RUL}_i$) at FT_i can be obtained as

$$\widetilde{RUL}_i = \underset{RUL_{P_i} \in RUL_i}{\operatorname{argmax}} f\left(RUL_{P_i}\right) \tag{8}$$

  where the $\operatorname{argmax}_{x \in S} f(x)$ represent arguments x for which $f(x)$ attains its largest value.

- For the failure threshold series FT:

  Each failure threshold contained in FT corresponds to a predicted RUL value as described above, and *h* predicted RUL values constitute a predicted RUL series $\widehat{RUL} = \left(\widetilde{RUL}_1, \widetilde{RUL}_2, \dots, \widetilde{RUL}_h\right) \in \mathbb{R}^h$.

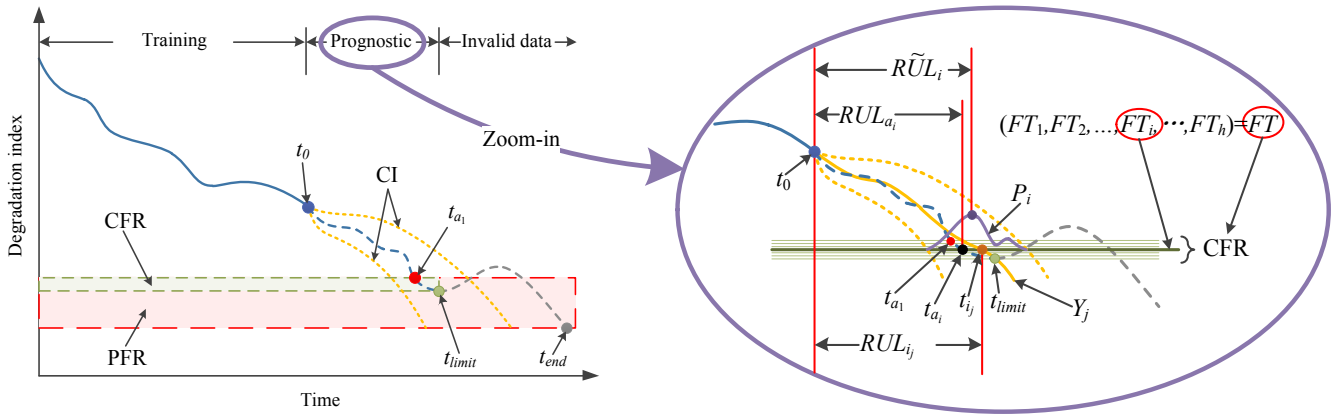

(a) (b)

Figure 4. Schematic of fusion prognostics:
(a) segmentation of degradation index (data set), and failure ranges;
(b) when prediction starting point is t_0, zoom-in prognostic part and predict remaining useful life.

For the sake of clarity, the main notation involved in Figure 4 and/or this subsection is summarized as follows.

t_0:	Specified prediction starting point;
t_{a_1}:	Expected earliest failure point, which is the cross point of FT_1 and DI;
t_{limit}:	Extreme point of recoverable fault;
t_{end}:	Data ending point;
CI:	Confidence interval of predictions;
PFR:	Probable failure range, which is between t_{a_1} and t_{end};
CFR:	Calculable failure range, which is between t_{a_1} and t_{limit};
Training:	Historical data, i.e., the training set, which is before point t_0;
Prognostic:	Future (unknown) data, i.e., test set, which is between t_0 and t_{limit};
Invalid data:	Data not available for prognostics, which is between t_{limit} and t_{end};
FT:	The h failure thresholds contained in the CFR;
FT_i:	An element from FT, which is the i-th failure threshold ($i = 1,2, \ldots, h$).
t_{a_i}:	Actual end-of-life at FT_i, i.e., the cross point of FT_i and DI;
Y_j:	The j-th ($j = 1,2, \ldots, l$) predicted degradation trend;
$\hat{Y}$:	A series of predicted degradation trends at FT_i, i.e., $\hat{Y} = (Y_1, \ldots, Y_j, \ldots, Y_l)$;
t_{i_j}:	The j-th predicted end-of-life at FT_i, i.e., the cross point of FT_i and Y_j;
RUL_{i_j}:	Predicted RUL corresponding to Y_j, i.e., $t_{i_j} - t_0$.
RUL_i:	A series of predicted RUL at FT_i, i.e., $RUL_i = (RUL_{i_1}, \ldots, RUL_{i_j}, \ldots, RUL_{i_l})$.
P_i:	The probability density distribution based on RUL_i;
$R\tilde{U}L_i$:	Final predicted RUL at FT_i, corresponds to the maximum of P_i;
RUL_{a_i}:	Actual RUL at FT_i, i.e., $t_{a_i} - t_0$.

4 Vehicle-oriented long-term accelerated stress test experiments

To validate properly the proposed fusion prognostics method, long-term dynamic ageing experimental data from a vehicle-oriented commercial PEMFC single cell is used [30]. Specifically, a test station with integrated control and observation is used to deploy the ageing experiment, and to activate the PEMFC before performing the test. The relative humidity of the cathode and anode is regulated by the built-in humidifier of the test station. A peripheral water-cooling system is used to handle the operating temperature of PEMFC. The main technical parameters of the PEMFC are listed in Table 2, where the cathode/anode inlet pressures and relative humidity, as well as the operating temperature, are set to the desired optimal values.

Table 2 Dynamic ageing test conditions

Items	Values
Active surface (cm^2)	25
Hydrogen inlet-pressure (KPa)	110
Air inlet-pressure (KPa)	110
Operating temperature (°C)	85
Hydrogen relative humidity (%)	50
Air relative humidity (%)	80
Full load current (A)	35.6
Load currents involved in dynamic load cycles (A)	0; 1.78; 4.45; 9.51; 10.4; 14.85; 20.75; 29.65

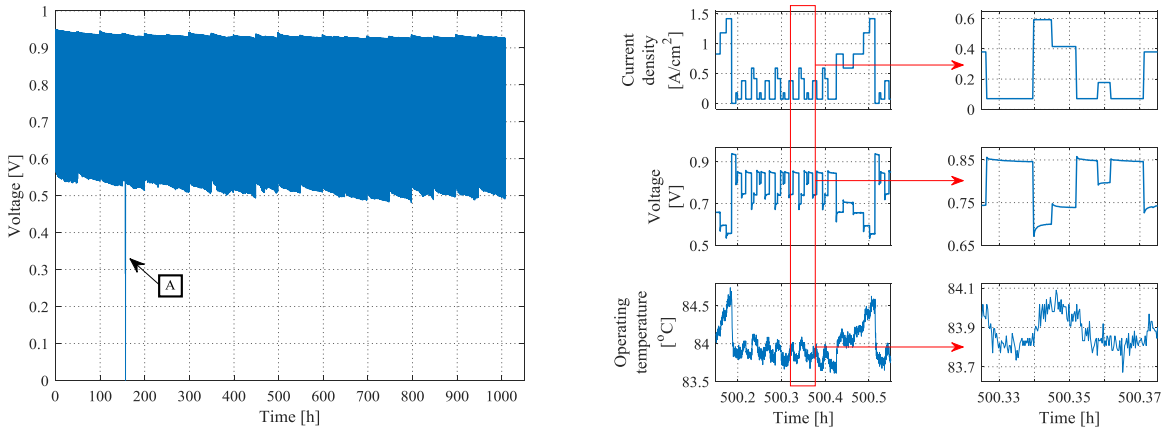

(a) (b)

Figure 5. Cyclic dynamic loading for accelerated stress testing:
(a) overall dynamic voltage;
(b) around 500 hours, current density, voltage and operating temperature in one cycle, and zoom-in details.

This ageing experiment can be considered as an In-situ accelerated stress test (AST) [24], which is designed with reference to the New European Driving Cycle (NEDC) [30]. As shown in Figure 5, each cycle lasts for 1,181 s, including the urban condition (performed 4 times) and the suburban condition (performed one time). Nine different load currents (0-100%) are involved as shown in Table 2. The entire ageing experiment consists of 3,076 cycles, accounting for approximately 1,008 hours. A polarization curve test is performed before the start of the overall ageing experiment. Subsequently, the AST is suspended every 50 hours and resumed until the end of the polarization curve test (non-shutdown). In addition, every 100 hours, a

planned shutdown of 12 hours is executed to simulate the shutdown-condition of the actual vehicle. It is worth mentioning that typically the shutdown comes with a performance recovery of the PEMFC. This is realistic, but it inevitably causes fluctuations in DI, making the prognostics challenging.

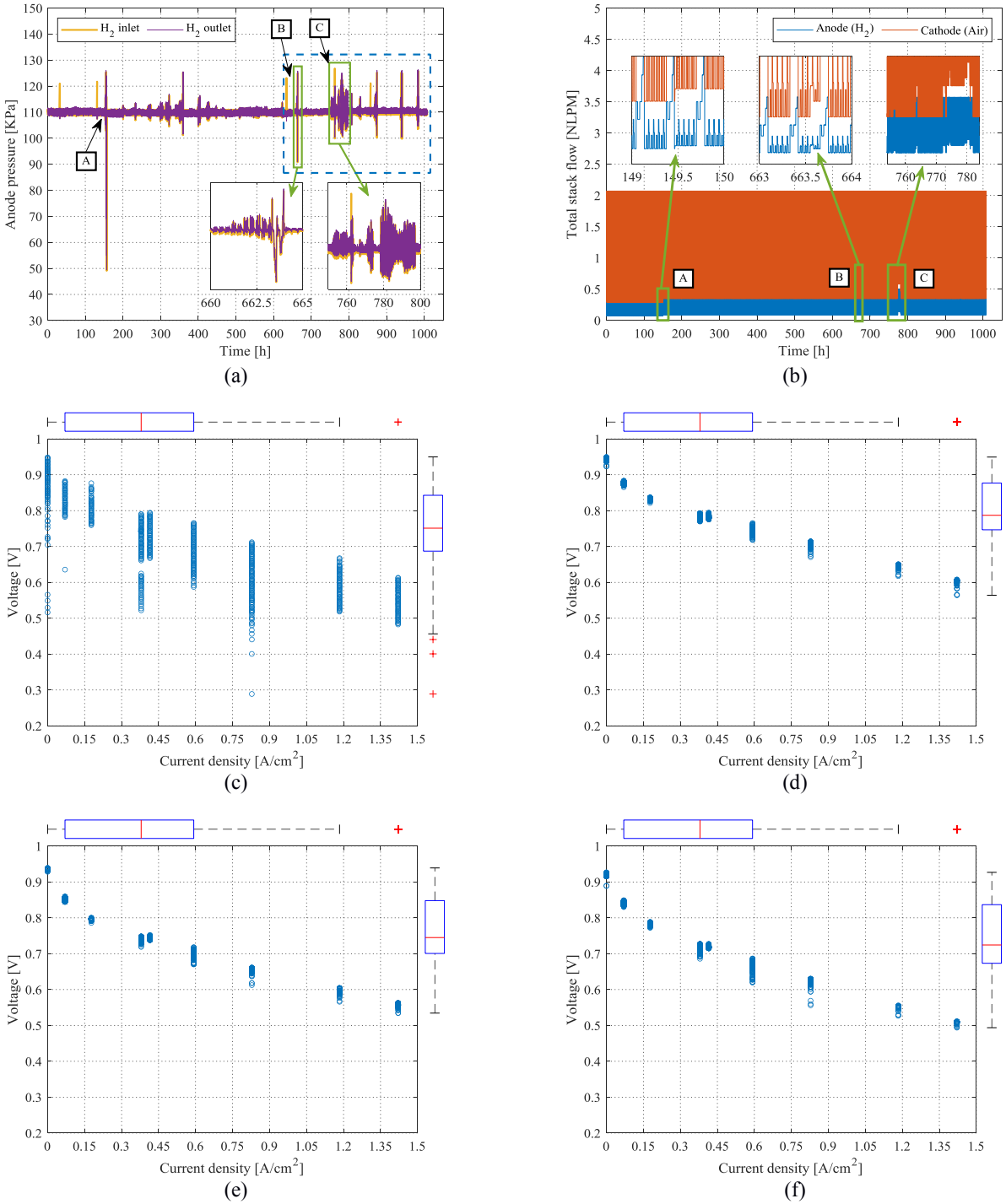

Figure 6. Anode gas pressure conditions and total stack flow,
(a) the relationship between anode gas pressure and abnormal operation;
(b) the relationship between total stack flow and abnormal operation;
Current density-voltage scatterplot in,
(c) overall (0-1008 hours); (d) 0-1 hours; (e) 500-501 hours; (f) 1007-1008 hours.

During the ageing experiments, the test station and peripheral equipment encounter some anomalies, which are referred to as abnormal operations in this paper. As in Figure 6(a), the inlet/outlet pressure of hydrogen is set at the optimal value of 110 KPa. However, significant fluctuations arise in practice. Coincidentally, as in Figure 6(b), the total stack flow of H_2/Air also exhibit the related abnormal operations. Among them,

- Point A is a sharp oscillation of the inlet pressure that occurred at around 150 hours, corresponding to the shutdown-like voltage dip in Figure 5(a).
- Point B is the frequent and more violent hydrogen supply anomalies starting at around 660 hours, as in the blue dashed box in Figure 6(a).
- Point C, some gas pressure/flow anomalies lasting more than 10 hours are observed during 750-800 hours.

More details of the experimental data can be found in [22,30].

Figure 6 (c) is the overall (0-1008 hours) current density-voltage scatterplot, which contains the long-term degradation and anomalous operations. The following phenomena are contained in Figure 6 (d)-(f), (1) ageing experiments with 9 different loads including full load, which covers most of the operating conditions. (2) the decrease in voltage with time, which reflects the degradation in performance; (3) unlike the typical polarization curve, the data points are more dispersive due to the inclusion of short-term (transient) dynamics. (4) The cell dynamic load operates mainly in the ohmic losses region. In these cases, the degradation model proposed in this paper can be used to handle the dynamics.

Remark: For most fuel cells, whether in the form of a single cell or a stack and regardless of the output power levels, it is recommended typically to operate in the ohmic losses region, which represents high efficiency. Recall that this work is based on single-cell modelling that can be extended to a stack. Therefore, the use of the above experimental data to verify the prognostic strategy does not limit its generality.

5 Prognostics results evaluation and discussion

5.1 Evaluation criteria

In this paper, two metrics are used to evaluate the hybrid prognostics method, relative error (RE) and prognostic horizon (PH). Among them, RE is given by

$$RE = \frac{|x - \hat{x}|}{x} \cdot 100\% \tag{9}$$

where x can be the actual single-cell voltage (E_{cell}) or the actual remaining useful life (RUL_{a_i}); $\hat{x}$ corresponds to the identified/reconstructed single-cell voltage ($\hat{E}_{cell}$) or the predicted remaining useful life ($\widetilde{RUL}_i$).

Subsequently, the predicted RUL is further evaluated using PH, the definition of which differs from those proposed in [29,31]. In this paper, PH is defined using a Trust Area (TA), which is the area between the upper/lower trustworthiness boundaries parallel to the actual RUL. In the CFR, the i-th ($i = 1,2,\ldots,h$) failure threshold FT_i corresponds to the TA_i and the PH_i as follows

$$\begin{cases} RUL_{a_i} - t_{a_i} \cdot \alpha_{low} \le TA_i \le RUL_{a_i} + t_{a_i} \cdot \alpha_{up} \\ PH_i = t_{a_i} - t_{1st_i} \end{cases} \tag{10}$$

where α_{low} and α_{up} are used to adjust the tolerance of TA_i, the smaller they are the tighter the Trust Area (and the smaller the range of TA_i). In this paper, α_{low} and α_{up} are set to 15% and 5%, respectively. t_{1st_i} denotes the earliest time point after which the predicted RULs are all within the TA_i. The larger PH is, the more sufficient time is guaranteed for control/maintenance and the more effective the prognostics.

5.2 Evaluation of extracted degradation index

Based on the analysis for the current density-voltage scatterplot in Section 4, in this paper, equal interval division is chosen for the DI extraction. The width of each time slot is set to the duration of three dynamic cycles (about one hour). In Table 3, the identified parameters are listed, along with the type of voltage losses to which they belong.

Table 3 Parameter identification results

Parameter	Value/Range	Overpotential losses
α_{a+c}	0.74	Activation
j_{loss} (mA/cm^2)	10	Activation
j_{exch} (mA/cm^2)	9	Activation
β_{a+c}	0.13	Concentration
j_{max} (A/cm^2)	3.539	Concentration
C_{dl} (mF/cm^2)	64 to 464	Activation & Concentration
R_{dyn} (Ωcm^2)	-0.007 to 0.053	Activation & Concentration
R_r (Ωcm^2)	0.03 to 0.08	Ohmic
R_{equ} (Ωcm^2)	0.0344 to 0.1002	Ohmic (nominal)
E_{rev} (V)	0.923 to 0.967	-

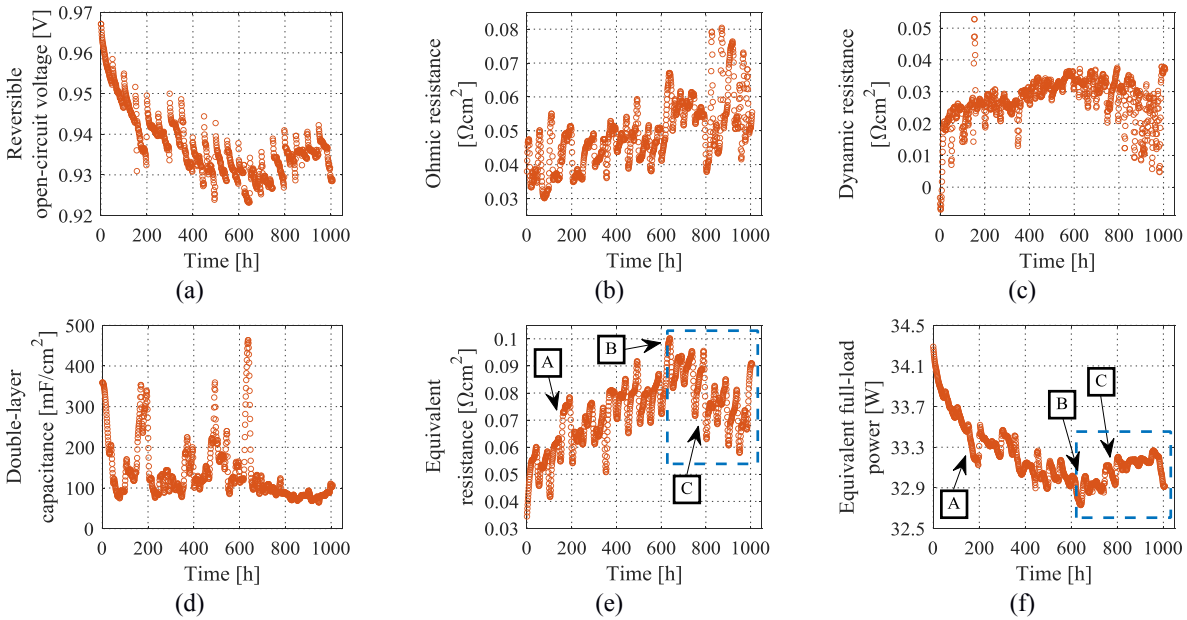

Figure 7. Parameters identification:
(a) reversible open-circuit voltage (E_{rev}); (b) Ohmic resistor (R_r); (c) dynamic resistor (R_{dyn});
(d) double-layer capacitor (C_{dl}). (e) equivalent resistance (R_{equ}); (f) equivalent full-load power (P_{equ}).

In Figure 7, the identified variable parameters are shown. By introducing all identified parameters into equations (1)-(3) and setting the operating current at 35.6 A, the equivalent full-load power (P_{equ}) is calculated and illustrated in Figure 7(f). In overall, almost all the variable parameters show a significant jump at point A, this is caused by a severe fault in the hydrogen supply. Meanwhile, there is a clear change of the trend after point B, which can be considered as an effect of the abnormal gas pressure/flow operation mentioned in Section 4 (Figure 6(a) and (b)). There are some obvious outlier points in C_{dl} and the trend characteristics are not obvious. In addition, all other variable parameters show different levels of trend characteristics until point B. To be specific, $E_{rev}$and P_{equ} appear to possess generally decreasing trends, but P_{equ} looks smoother. R_r, R_{dyn} and R_{equ} imply generally increasing trends, with R_{equ} showing a more clearly monotonous trend. Moreover, considering that both R_{equ} and P_{equ} are the parameters that characterize the overall situation with physical interpretation, they are designated as DI_1 and DI_2, respectively. It is worth mentioning that the trend features inherent in the identified parameters are consistent with the experimental data or have physical interpretability. Moreover, some parameters are not selected as DIs, but they can still be potential candidates. For instance, the trend feature of C_{dl} is not obvious, but its outliers indicate some abnormal operation of the fuel cell.

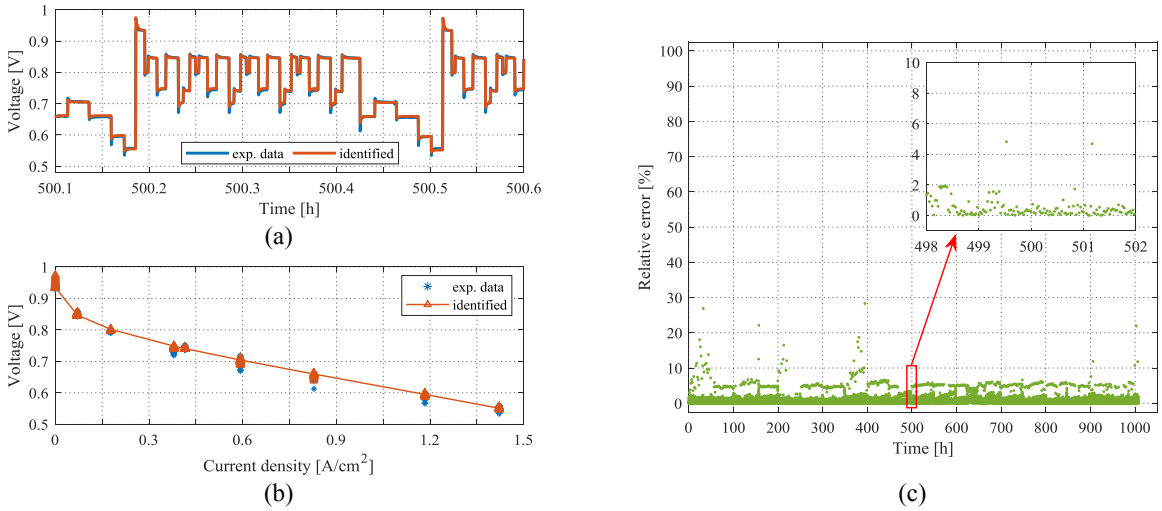

Figure 8. Evaluation of dynamic load identification performance:
(a) identification of the cell voltage;
(b) current density-voltage plot of identification results;
(c) relative error of identification results.

The final output of the degradation mechanism model is the single cell voltage. Thus, the cell voltage values calculated by the identified model are compared with the actual measurements to evaluate the model identification performance. As an example, Figure 8 (a) and (b) show the comparison corresponding to a dynamic cycle around 500 hours. Figure 8 (a) shows that the operating voltages and the reconstructed voltages which can match well to each other. Figure 8 (b) shows the current density-voltage plot in which the overall match is satisfactory. It is worth noting that, after load switching, as in Figure 5(b), the voltage exhibits an overshoot-like dynamic. Especially at the instants of switching, such dynamics correspond to the points in Figure 8(b) where the experimental data are out of the identification curve. At these points, the reconstructed voltage fitting performance is slightly worse. That is because, as mentioned in Section 2, simplifications are considered when modelling the degradation mechanism. Furthermore, to quantitatively evaluate the model performance, the relative error (RE_E) in terms of single-cell voltage is calculated using equation (9) and illustrated in Figure 8(c). Observations for the ageing test are sampled at 1 Hz, so the RE_E

is calculated over more than 3.6 million data points. The average RE_E is less than 1%, which demonstrates the effectiveness of the proposed model and model identification method.

5.3 Evaluation of predicted remaining useful life

In evaluating the performance of the proposed RUL prediction method, the prediction starting points and failure range are set based on the analysis of DI_1 and DI_2, as in Figure 9. In particular, a change in operational behaviour after point B is considered. As a consequent change in the degradation trend is observed after B, the DI after the maximum/minimum point near B (approximately hour 640) is set as invalid. For the useful DI, RUL predictions are deployed at 50-hour intervals from about 50 hours to about 500 hours. Meanwhile, a CFR consisting of a series of failure thresholds is set in place of a single failure threshold. For DI_1, the CFR is 0.0961-0.1001 Ωcm^2 ; while the CFR for DI_2 is set to 32.74-32.82 W.

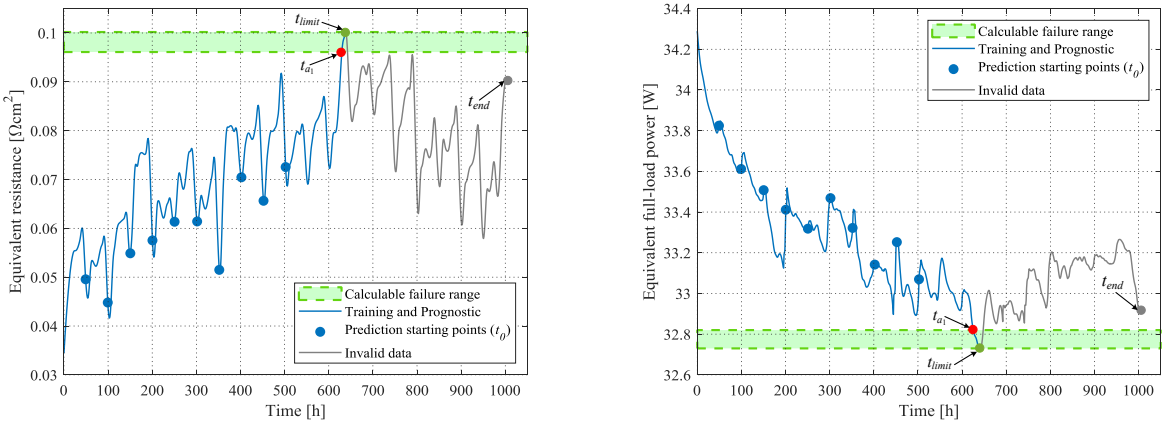

(a) (b)

Figure 9. Degradation index and failure range for prognostics:
(a) equivalent resistance (DI_1);
(b) equivalent full-load power (DI_2).

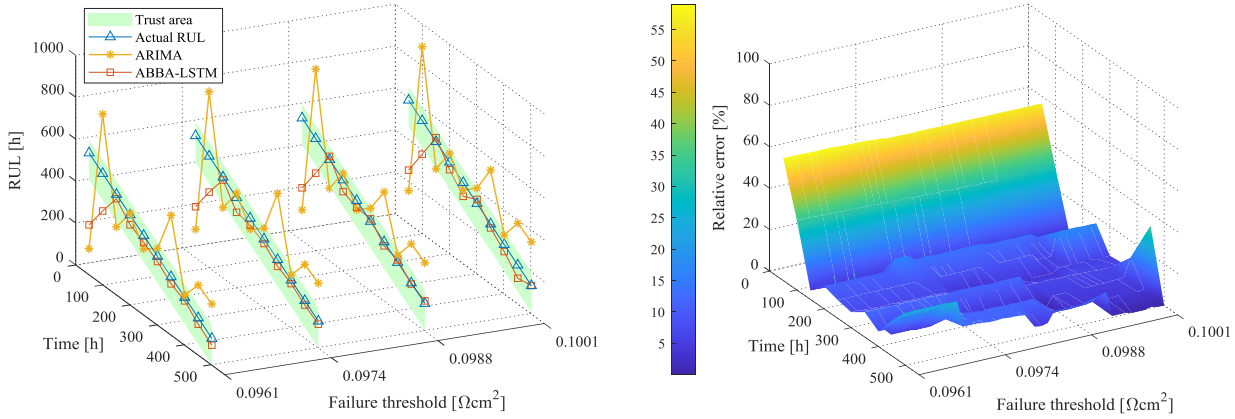

(a) (b)

Figure 10. For DI_1, RUL prediction performance and evaluation at different failure thresholds (FTs):
(a) comparison experiments and prognostic horizon evaluation;
(b) relative error of the CFR (0.0961-0.1001 Ωcm^2).

For DI_1, the performance of the proposed method in terms of RUL prediction is evaluated as shown in Figure 10. In the first two test points, the predicted RUL does not enter the TA. This is mainly because the training data in the early stage are not sufficient to capture the global evolution trend. With increased training

data, the prediction error gradually decreases and predicted RUL enters the TA. The calculated PH exceeds 350 hours on different FTs. If the full useful lifetime is set to 640 hours, this means that the PH exceeds 50% of it. In addition, to evaluate more appropriately the prognostic performance, comparison experiments are deployed using the Autoregressive Integrated Moving Average (ARIMA) model. As in Figure 10(a), some prediction results of the ARIMA model exhibit greater errors compared to the ABBA-LSTM. In terms of consistency, the two models perform similarly. On the other hand, in Figure 10 (b), the prediction performance is quantitatively evaluated using equation (9). Overall, the prediction errors maintain high stability when FT varies. Moreover, the average relative error in the CFR is 15.5%.

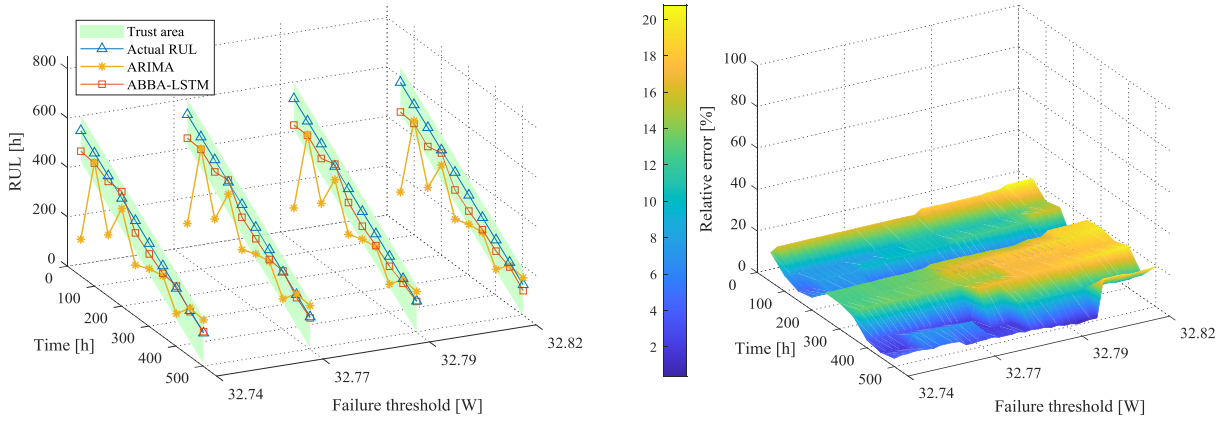

(a) (b)

Figure 11. For DI_2, RUL prediction performance and evaluation at different failure thresholds (FTs):
(a) comparison experiments and prognostic horizon evaluation;
(b) relative error of the CFR (32.74-32.82 W).

The same performance evaluation is deployed on DI_2, as in Figure 11. Thanks to DI_2 being smoother, the prediction performance is better than DI_1 overall. For different FTs, PHs are greater than 400 hours which accounts for more than 60% of the full useful lifetime. In the best case, PH exceeds 450 hours, which means that satisfactory prognostic results can be given with only 50 hours of ageing data. Additionally, in the comparison experiments, as in Figure 11(a), almost all the predictions of the ARIMA model are lower than the actual RUL, and most of them perform worse than the ABBA-LSTM. On the other hand, the performance of the relative error is stable within the CFR. Then the average relative error in the CFR is 11.4%.

5.4 Discussion

The RUL predictions based on DI_1 and DI_2 are not entirely consistent, especially at the earliest two "prediction start points". This result can be attributed to the following factors.

(1) Generally, RUL prediction precision is related to the size of the historical dataset. The prediction results based on DI_1 and DI_2 are limited by the training set size at the initial "prediction start points", thus the performances are not satisfactory.

(2) Overall, the fluctuation of DI_1 is larger than that of DI_2. After superimposing the limitation of the training data size, the prediction performance based on DI_1 is worse in the earliest two prediction points.

(3) As more data are available for training the model, the predictions gradually converge to the actual RUL. For both DIs, since the third "prediction start point", the predictions almost all fall in the trust area.

(4) The ARIMA model used for performance comparison also exhibits the above characteristics, although its performance is inferior to that of the ABBA-LSTM in general.

6 Conclusion

In this work, a fusion prognostics strategy is proposed for predicting the remaining useful life of fuel cells. A degradation mechanism model is used to handle the dynamic operating conditions of FC and extract the degradation indexes that can be used for prognostics. In addition, the proposed method is validated using the accelerated stress test/dynamic load cycle ageing test data of a vehicle-oriented PEMFC. The results show that the proposed degradation mechanism model can effectively track both the dynamics caused by load transitions and the ageing-related parameter variation. The average relative error of the model output is less than 1%. Furthermore, two different degradation indexes, i.e., equivalent resistance and full power, are extracted and the ABBA-LSTM RUL prediction model is evaluated in the set failure region of the two degradation indexes respectively. The results show that the prognostic horizon that exceeds 60% of the useful full lifetime can be achieved, and the relative error of RUL prediction can reach 11.4%. The proposed fusion strategy has the ability to handle long-term prognostics that are full of dynamics in automobile applications. In the future work, we aim to identify and remove the unnatural ageing component of the degradation index, as well as combine multiple degradation indexes appropriately to improve the ageing prognostic performance.

Acknowledgement

This work was supported in part by the China Scholarship Council (CSC) under Grant [grant number 201906290107].

Appendix A

In general, the refined choice of filter $L(s)$ is used to cope with the disturbances embedded in the system when estimating the system variables [32].

$$L(s) = \frac{1}{A(s)} \tag{A.1}$$

In fact, $A(s)$ is the denominator of $H(s)$, for which the unknown part is replaced by the estimated value. Based on this, the following equation is obtained after filtering equation (4).

$$\begin{aligned} L(s)v'(t) &= -a_1 L(s)v(t) + b_1 L(s)j'(t) + b_2 L(s)j(t) + L(s)e(t) \\ &= \varphi^T(t)\theta + L(s)e(t) \end{aligned} \tag{A.2}$$

where $v'(t)$ and $j'(t)$ correspond to the first order derivatives of the variables, $e(t)$ is the disturbance of the system, and $\varphi(t)$ and θ are as follows,

$$\begin{cases} \varphi(t) = [-L(s)v(t)\ ,\ L(s)j'(t)\ ,\ L(s)j(t)]^T \\ \theta = [a_1\ ,\ b_1\ ,\ b_2]^T \end{cases} \tag{A.3}$$

Considering that typically $e(t)$ is not necessarily white noise, the Instrumental Variable (IV) method is chosen in order to reduce the estimation bias. The predicted output $\hat{v}(t)$ will constitute the instrument vector $\zeta(t)$,

$$\zeta^T(t) = [-L(s)\hat{v}(t) \ , \ L(s)j'(t) \ , \ L(s)j(t)] \tag{A.4}$$

The parameters are subsequently estimated using the following equation,

$$\hat{\theta} = \left[\sum_{i=1}^{N} \zeta^T(t_i)\varphi(t_i)\right]^{-1} \sum_{i=1}^{N} \zeta^T(t_i)[L(s)v'(t_i)] \tag{A.5}$$

where $\hat{\theta}$ represents the estimated parameters [32].

References

[1] Ramsden T. 2019 Annual Progress Report: DOE Hydrogen and Fuel Cells Program. United States; 2020. https://www.osti.gov/biblio/1660255.

[2] European Commission. A hydrogen strategy for a climate-neutral Europe. Brussels (BE); 2020. https://ec.europa.eu/energy/sites/ener/files/hydrogen_strategy.pdf.

[3] Yue M, Jemei S, Gouriveau R, Zerhouni N. Review on health-conscious energy management strategies for fuel cell hybrid electric vehicles: Degradation models and strategies. Int J Hydrogen Energy 2019;44(13):6844-61. https://doi.org/10.1016/j.ijhydene.2019.01.190.

[4] Hao X, Yuan Y, Wang H, Ouyang M. Plug-in hybrid electric vehicle utility factor in China cities: Influencing factors, empirical research, and energy and environmental application. eTransportation 2021;10:100138. https://doi.org/10.1016/j.etran.2021.100138.

[5] Hu Z, Xu L, Li J, Ouyang M, Song Z, Huang H. A reconstructed fuel cell life-prediction model for a fuel cell hybrid city bus. Energy Convers Manag 2018;156:723-32. https://doi.org/10.1016/j.enconman.2017.11.069.

[6] Peng H, Chen Z, Deng K, Dirkes S, Ünlübayir C, Thul A, et al. A comparison of various universally applicable power distribution strategies for fuel cell hybrid trains utilizing component modeling at different levels of detail: From simulation to test bench measurement. eTransportation 2021;9:100120. https://doi.org/10.1016/j.etran.2021.100120.

[7] Pfeifer A, Prebeg P, Duić N. Challenges and opportunities of zero emission shipping in smart islands: A study of zero emission ferry lines. eTransportation 2020;3:100048. https://doi.org/10.1016/j.etran.2020.100048.

[8] Gao W, Hu Z, Huang H, Xu L, Fang C, Li J, et al. All-condition economy evaluation method for fuel cell systems: System efficiency contour map. eTransportation 2021;9:100127. https://doi.org/10.1016/j.etran.2021.100127.

[9] Jouin M, Gouriveau R, Hissel D, Péra M-C, Zerhouni N. Degradations analysis and aging modeling for health assessment and prognostics of PEMFC. Reliab Eng Syst Saf 2016;148:78-95. https://doi.org/10.1016/j.ress.2015.12.003.

[10] Jacome A, Hissel D, Heiries V, Gerard M, Rosini S. Prognostic methods for proton exchange membrane fuel cell under automotive load cycling: a review. IET Electr Syst Tran 2020;10(4):369-75. https://doi.org/10.1049/iet-est.2020.0045.

[11] Sutharssan T, Montalvao D, Chen Y K, Wang W-C, Pisac C, Elemara H. A review on prognostics and health monitoring of proton exchange membrane fuel cell. Renew Sustain Energy Rev 2017;75:440-50. https://doi.org/10.1016/j.rser.2016.11.009.

[12] ISO 13381-1:2015. Condition monitoring and diagnostics of machines - prognostics - Part 1: General Guidelines. International Organization for Standardization 2015. https://www.iso.org/standard/51436.html.

[13] Liu H, Chen J, Hissel D, Lu J, Hou M, Shao Z. Prognostics methods and degradation indexes of proton exchange membrane fuel cells: A review. Renew Sustain Energy Rev 2020;123:109721. https://doi.org/10.1016/j.rser.2020.109721.

[14] Ma R, Li Z, Breaz E, Liu C, Bai H, Briois P, et al. Data-Fusion Prognostics of Proton Exchange Membrane Fuel Cell Degradation. IEEE Trans Ind Appl 2019;55(4):4321-31. https://doi.org/10.1109/tia.2019.2911846.

[15] Wang C, Li Z, Outbib R, Zhao D, Dou M. Proton Exchange Membrane Fuel Cells Prognostic Strategy Based on Navigation Sequence Driven Long Short-term Memory Networks. IECON 2020 The 46th Annual Conference of the IEEE Industrial Electronics Society 2020:3969-74. https://doi.org/10.1109/IECON43393.2020.9255373.

[16] Wang F K, Cheng X B, Hsiao K C. Stacked long short-term memory model for proton exchange membrane fuel cell systems degradation. J Power Sources 2020;448: 227591. https://doi.org/10.1016/j.jpowsour.2019.227591.

[17] Bressel M, Hilairet M, Hissel D, Ould-Bouamama B. Remaining Useful Life Prediction and Uncertainty Quantification of Proton Exchange Membrane Fuel Cell Under Variable Load. IEEE Trans Ind Electron 2016;63(4):2569-77. https://doi.org/10.1109/tie.2016.2519328.

[18] Mezzi R, Yousfi-Steiner N, Péra M C, Hissel D, Larger L. An Echo State Network for fuel cell lifetime prediction under a dynamic micro-cogeneration load profile. Appl Energy 2021;283:116297. https://doi.org/10.1016/j.apenergy.2020.116297.

[19] Li Z, Jemei S, Gouriveau R, Hissel D, Zerhouni N. Remaining useful life estimation for PEMFC in dynamic operating conditions. 2016 IEEE Vehicle Power and Propulsion Conference (VPPC) 2016:1-6. https://doi.org/10.1109/VPPC.2016.7791762.

[20] Li Z, Zheng Z, Outbib R. Adaptive Prognostic of Fuel Cells by Implementing Ensemble Echo State Networks in Time-Varying Model Space. IEEE Trans Ind Electron 2020;67(1):379-89. https://doi.org/10.1109/tie.2019.2893827.

[21] Yue M, Li Z, Roche R, Jemei S, Zerhouni N. A Feature-based Prognostics Strategy for PEM Fuel Cell Operated under Dynamic Conditions. 2020 Prognostics and Health Management Conference (PHM-Besançon) 2020:122-7. https://doi.org/10.1109/PHM-Besancon49106.2020.00026.

[22] Zuo J, Lv H, Zhou D, Xue Q, Jin L, Zhou W, et al. Deep learning based prognostic framework towards proton exchange membrane fuel cell for automotive application. Appl Energy 2021;281:115937. https://doi.org/10.1016/j.apenergy.2020.115937.

[23] Wang C, Li Z, Outbib R, Dou M, Zhao D. Symbolic deep learning based prognostics for dynamic operating proton exchange membrane fuel cells. Appl Energy 2022;305:117918. https://doi.org/10.1016/j.apenergy.2021.117918.

[24] Zhao J, Li X. A review of polymer electrolyte membrane fuel cell durability for vehicular applications: Degradation modes and experimental techniques. Energy Convers Manag 2019;199:112022. https://doi.org/10.1016/j.enconman.2019.112022.

[25] Asensio F J, San Martín J I, Zamora I, Saldaña G, Oñederra O. Analysis of electrochemical and thermal models and modeling techniques for polymer electrolyte membrane fuel cells. Renew Sustain Energy Rev 2019;113:109283. https://doi.org/10.1016/j.rser.2019.109283.

[26] Qi Y, Espinoza-Andaluz M, Thern M, Li T, Andersson M. Dynamic modelling and controlling strategy of polymer electrolyte fuel cells. Int J Hydrogen Energy 2020;45(54):29718-29. https://doi.org/10.1016/j.ijhydene.2019.09.178.

[27] O'hayre R, Cha S-W, Colella W, Prinz F B. Fuel cell fundamentals. John Wiley & Sons, 2016. https://doi.org/10.1002/9781119191766.

[28] Elsworth S, Güttel S. Time series forecasting using LSTM networks: A symbolic approach. arXiv preprint arXiv:2003.05672, 2020. https://arxiv.org/abs/2003.05672.

[29] Jouin M, Bressel M, Morando S, Gouriveau R, Hissel D, Péra M-C, et al. Estimating the end-of-life of PEM fuel cells: Guidelines and metrics. Appl Energy 2016;177:87-97. https://doi.org/10.1016/j.apenergy.2016.05.076.

[30] Zuo J, Lv H, Zhou D, Xue Q, Jin L, Zhou W, et al. Long-term dynamic durability test datasets for single proton exchange membrane fuel cell. Data Brief 2021;35:106775. https://doi.org/10.1016/j.dib.2021.106775.

[31] Saxena A, Celaya J, Balaban E, Goebel K, Saha B, Saha S, et al. Metrics for evaluating performance of prognostic techniques. 2008 International Conference on Prognostics and Health Management 2008:1-17. https://doi.org/10.1109/PHM.2008.4711436.

[32] Ljung L. Experiments with identification of continuous time models. IFAC Proceedings Volumes 2009;42(10):1175-80. https://doi.org/10.3182/20090706-3-FR-2004.00195.

[33] Huang Z, Shen J, Chan S H, Tu Z. Transient response of performance in a proton exchange membrane fuel cell under dynamic loading. Energy Convers Manag 2020;226:113492. https://doi.org/10.1016/j.enconman.2020.113492.

[34] Gong C, Shen J, Yu Y, Wang K, Tu Z. A novel radiator structure for enhanced heat transfer used in PEM fuel cell vehicle. Int J Heat Mass Transf 2020;157:119926. https://doi.org/10.1016/j.ijheatmasstransfer.2020.119926.

[35] Chen B, Cai Y, Tu Z, Chan S H, Wang J, Yu Y. Gas purging effect on the degradation characteristic of a proton exchange membrane fuel cell with dead-ended mode operation I. With different electrolytes. Energy 2017;141:40-9. https://doi.org/10.1016/j.energy.2017.09.067.

[36] Wang C, Li Z, Outbib R, Dou M, Zhao D. A novel long short-term memory networks-based data-driven prognostic strategy for proton exchange membrane fuel cells. Int J Hydrogen Energy 2022;47(18):10395-408. https://doi.org/10.1016/j.ijhydene.2022.01.121.

[37] Zhang Z, Wang YX, He H, Sun F. A Short- and Long-Term Prognostic Associating with Remaining Useful Life Estimation for Proton Exchange Membrane Fuel Cell. Appl Energy 2021;304:117841. https://doi.org/10.1016/j.apenergy.2021.117841.

[38] Ma R, Xie R, Xu L, Huangfu Y, Li Y. A Hybrid Prognostic Method for PEMFC with Aging Parameter Prediction. IEEE T Transp Electr 2021;7(4):2318-31. https://doi.org/10.1109/TTE.2021.3075531.

[39] Yue M, Li Z, Roche R, Jemei S, Zerhouni N. Degradation identification and prognostics of proton exchange membrane fuel cell under dynamic load. Control Eng Pract 2022;118:104959. https://doi.org/10.1016/j.conengprac.2021.104959.